Open Access

Journal of Energy and Power Technology

LIDSEN Publishing Inc.

Research Article

An 800V End to End SiC Powertrain to Accommodate Extremely Fast Charging

Naireeta Deb [1], Rajendra Singh [1, 2, *]

1. Holcombe Department of Electrical and Computer Engineering, Clemson University, Clemson, SC 29631, USA; E-Mails: ndeb@clemson.edu; srajend@clemson.edu
2. Department of Automotive Engineering, Clemson University, Clemson, SC 29631, USA

* **Correspondence:** Rajendra Singh; E-Mail: srajend@clemson.edu

Academic Editor: Mariano Alarcón

Special Issue: Sustainable and Safe Mobility

Journal of Energy and Power Technology
2023, volume 5, issue 1
doi:10.21926/jept.2301007

Received: November 15, 2022
Accepted: January 25, 2023
Published: February 08, 2023

Abstract

Widespread adoption of electric vehicles has presented the challenges of short range and prolonged charging time. Going forward, extremely fast charging is the only solution to these problems. However, the typical Silicon power electronics supported 400 V electric vehicle powertrain cannot live up to this challenge. Limitations include the huge cable size, heating of equipment due to high current and user safety, to name a few. In this paper, we have analyzed an 800 V EV powertrain using power electronics based on silicon carbide. In order to implement 800 V powertrain, the complete reconsideration of the electrical system is imperative. In this paper we have presented the implementation of Silicon Carbide based Power electronics to operate an 800 V powertrain and evaluate it against the 800 V Si powertrain. Details of drivetrain, inverter, and auxiliary power units in high voltage charging (Megawatt Level) system are presented in this research.

Keywords

Power electronics; silicon carbide; powertrain; extremely fast charging

1. Introduction

The sea level is rising because of the emission of harmful greenhouse gases. Studies suggest that earth is in the middle of the fifth mass extinction solely enabled by the greenhouse gas (GHG) produced by humanity [1]. An unusual heat wave is already almost upon all the countries [1]. The mobility industry plays a vital role in global economy. It enables trillions of dollars in trade every year. It is also the most significant source of avoidable GHG emission contributing almost 19% of the total GHG emissions [2]. This disaster is avoidable by adopting renewable energy and integrating it with energy storage devices such as batteries and changing the transportation industry to electric only [2]. The economic consequences will be significant to transform a heavily fossil fuel driven economy as the current grid is heavily dependent on fossil fuels. This means replacing the entire infrastructure. The oil producing countries will lose their revenue source and create turbulence in the industry. Oil has long been used as a geopolitical weapon [3]. Electrification of almost everything is the only solution to handle climate emergency [4]. As shown in Figure 1, by 2050 Internal combustion engine is expected to be replaced by EVs [5].

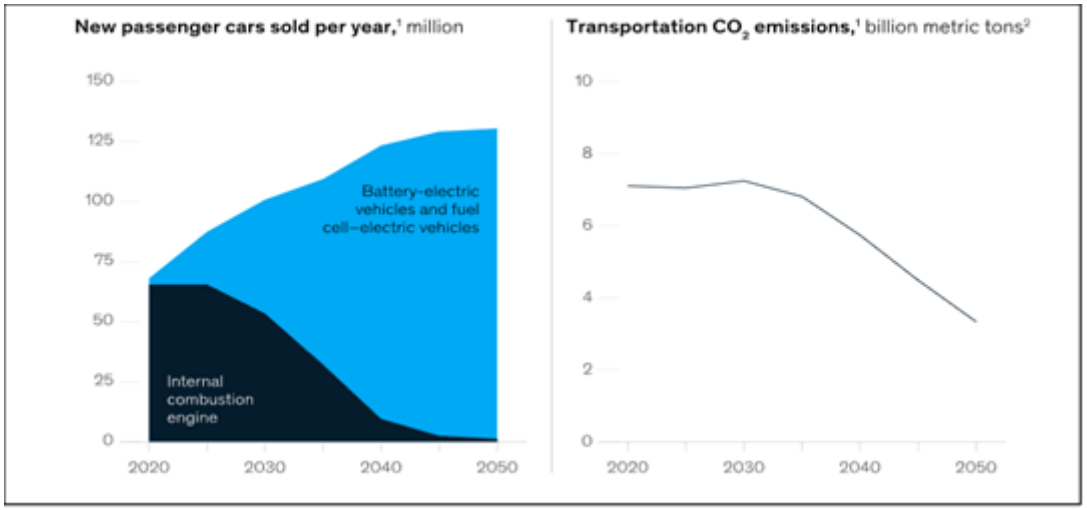

Figure 1 Car sales every year in ICEV and EV category [5].

The adaptation of electric vehicles around the world is very clear as the EV sales more than doubled in 2021 [6]. Bloomberg news reports that the world's EV fleet will soon surpass 20 million [7]. The revolution is led by China and Europe with USA a distant third [7]. In author's recent review paper, we thoroughly reviewed the roadblocks and cited the possible avenues to implement a green charging infrastructure for electric vehicles [8]. In United States, the adoption of EVs is discouraged by the efficiency of fossil-fueled vehicle's fast refueling experience and the reservation towards 100% green power generation, unlike Europe and China [5]. To overcome these barriers a silicon carbide power electronics based green charging infrastructure is proposed [8]. In order to increase the overall system energy efficiency, replacement of Si operated powertrain must be implemented for keeping up to the higher-power charging infrastructure. It must be noted, only increasing the charging power levels is futile if the EV itself has a low power drivetrain which is incapable of accepting the high-power charging. Clearly, these issues go hand in hand. According to recent data, a typical high-end battery electric vehicle (BEV) like Tesla Model S has a range of 405 miles. With Tesla Supercharger of 135 kW, this means a charging time of 27 to 40 minutes is estimated for the

400 V silicon power electronics-based power drivetrain. Whereas, refueling an IC Engine Vehicle (ICEV) will only take 5-10 mins. This discourages customers to adapt to EVs due to range anxiety. In recent paper, authors discussed 500 kW-1.2 GW level of charging being possible with SiC power electronics-based charging infrastructure, however the EV simply cannot accept the high level of charging with a 400 V drivetrain. The cable limitations must be incorporated while calculating the charging time as faster charging will increase the current rating by three to six times, conduction loss is the square of current rating meaning anywhere between nine to thirty-six times making the cable bulky and necessitating a costly cooling system to avoid an overheating explosion [9]. Therefore, the voltage rating of the powertrain must be increased to avoid an increase in current rating of the powertrain to avoid aforementioned limitations. Apart from reducing the current limit a high voltage powertrain will provide benefits including but not limited to battery current limit remaining same but charging getting faster, lower I^2R losses, smaller current rating in motor reducing their size. A set of publications that discuss 800 V powertrain has been reviewed in the literature [10-13]. However a complete evaluation of fully SiC powertrain against a fully Si Powertrain of similar voltage level is necessary, and this paper fills the gap in recent research.

Figure 2 shows the architecture of a BEV powertrain where the high-power battery is the main source of power that provides for the electric motor and a control unit that supplies power to the internal sub-systems. The motor is the high-voltage (HV) load, and the accessories are the low voltage loads. An in-depth analysis of this will be done in the next sections of this paper. However, the battery voltage level for most of the passenger cars today are 250-450 V. If we employ an 800 V system, the system must be adaptable to the new voltage levels; hence, power electronics play the most crucial role.

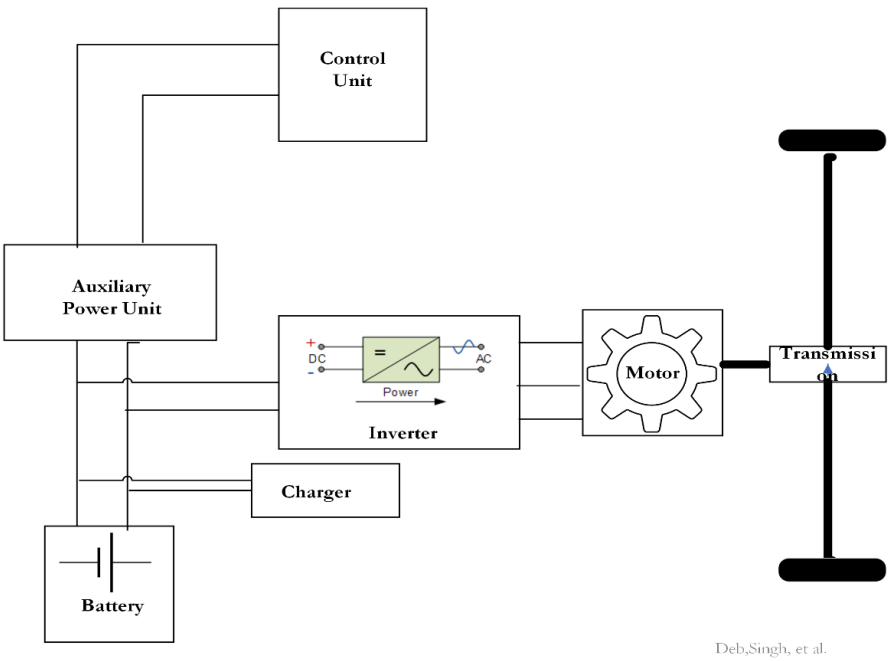

Figure 2 Typical Structure of a BEV Powertrain.

A comparative study of the physical properties of the devices (Si and SiC) in Table 1, gives an idea of its higher efficiency, lower loss and overall reduced weight thus making the Powertrain more efficient [12].

Table 1 Comparison of Physical Properties of Si & SiC for APU [12].

Properties	Si	SiC
Energy Gap(eV)	1.17	3.12
Electron Mobility(μn)	1700	980
Thermal Conductivity (W/cm.°C)	1.5	4.9
Saturation Drift Velocity vs. (cm/s)	1	2.2
Relative Dielectric Constant: ϵ_s	12.4	10.1
Breakdown Field: E_B (V/cm)	0.3	3

The paper is organized as follows. The next section selects appropriate power electronics device for evaluation. Section 3 explains the modelling approach and in Section 4, we have evaluated the impact of higher voltage battery energy storage system (BESS). In Section 5, we have explained the importance of power electronics in Powertrain. Section 6 covers the motor output improvement by using SiC based power electronics. Section 7 and 8 gives a brief overview of mechanical stress and charger in EV. Section 9 evaluates the auxiliary power unit in powertrain. Conclusion of the paper is given in section 10.

2. Parameter Selection

The parameter selection is pivotal element in this research and authors researched a multitude of automotive MOSFETs currently available in the market to select the top two candidates for analysis. The SiC MOSFET is UnitedSiC UF3C170400K3S [14] and the Si MOSFET [15] is Infeneon IPD80R2k7C3A. The devices were selected because in both categories the highest power device applicable for transportation electronics must be selected to compare at their optimum operating points. The core model will be replaced with these two devices enabled boards and results will be analyzed. The key parameters are listed below in Table 2.

Table 2 Parameter Selection.

Symbol	Attribute	Si Infeneon IPD80R2k7C3A [14]	SiC UnitedSiC UF3C170400K3S [15]
I_{DON}	On Current	6 A	14 A
R_{DSON}	On Resistance	2.7 Ω	410 mΩ
tr	Rise Time	15 nS	13 nS
tf	Fall Time	18 nS	27 nS
V_{DD}	Working Voltage	800 V	1700 V
D	Duty Cycle	50%	50%
f_{sw}	Switching Frequency	100 kHz	100 kHz
t_{off}	Off Time	72 nS	34 nS

3. Modelling

The modelling approach is based on reference [16], which represents every subsystem in equation blocks. The equation blocks are connected through signal blocks that are updated at every time step. In every subsequent section, the working equations will be presented and analyzed. The overview of the notional model is given in the simplified block diagram in Figure 3.

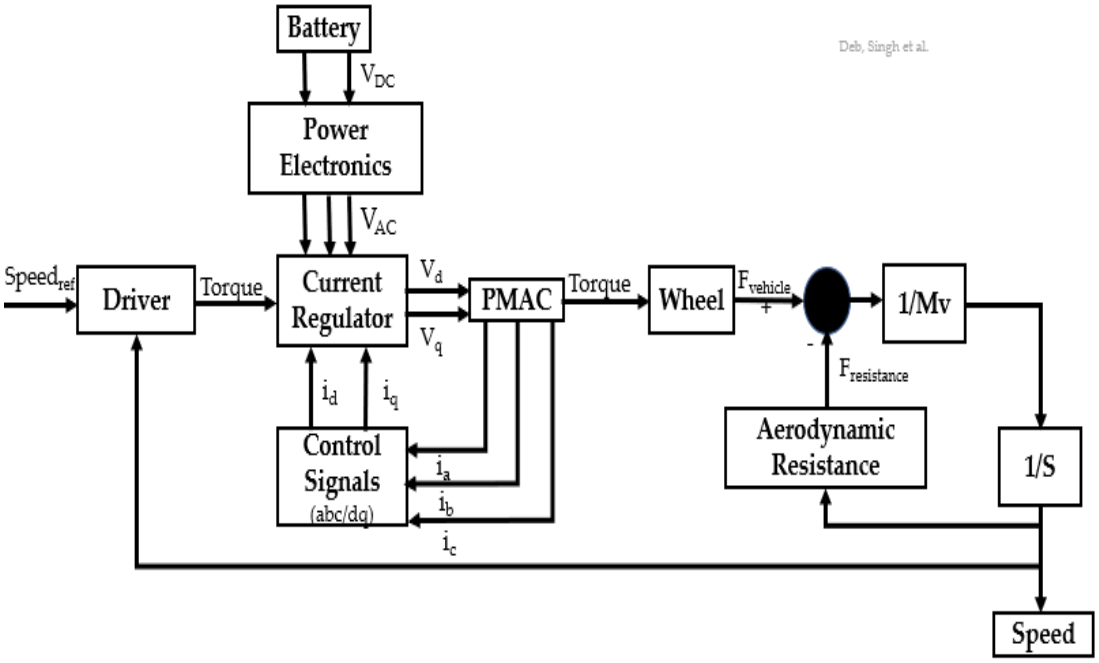

Figure 3 Simplified block diagram of the equation model.

4. Battery Energy Storage System (BESS)

With the emergence of EV revolution, researchers keep developing energy dense batteries. However, developing a high-performance battery without adequate conversion system is futile. In order to find the suitable battery system for an 800 V powertrain the key parameters of evaluation are energy density, power density, cycle life, calendar life and price/kWh [17]. Safety and volume are also crucial requirements for battery manufacturers.

Energy efficiency and self-discharge needs to be considered in a detailed level before approving a model [17]. Although the battery size is determined by the energy to be delivered to the powertrain, it must be mentioned that the equation representing relationship between car range and battery density is a complex one instead of a linear equation. The higher the battery weighs (range 150 kg-500 kg) the lesser the system efficiency. This in turn affects the power electronics design of the system too. Automotive MOSFET and IGBT manufacturers have been constant suppliers of Si based 650 V devices for the circuit board development of powertrain. Typically 96 Li-ion cells are connected in series, each having a voltage rating of 4.2 volts [10]. Therefore the peak output remains 403.2 V. Which is compatible with the 650 V peak power transistors being used in typical drivetrains. This has worked well so far for the typical 50 kW DC fast chargers. However, with increasing charging levels the current rating of the cables keeps increasing hence encouraging to use the 800 V battery packs.

The latest cooling techniques make the cable rating around 500 A without compromising the weight. The cable also needs to be flexible enough to be handled by the EV owner. Hence the cooling of charging cables go hand in hand with the battery sizing of powertrain.

In this paper we have considered two 800 V buses. The 800 V Si is notional whereas the 800 V SiC is akin to the Porche Taycan. The industry model of 400 V Si Powertrain was used as a reference to create the 800 V Si bus. Porche Taycan can charge in 18 minutes for the SoC of 5%-80% but the range is 212 km whereas the 400 V industry models such as Tesla model 3 has a range of 360 km [11]. It must be noted that the two companies mentioned above utilize different design perspectives in their powertrain model apart from the design of Power Electronics [12].

The industry models of 400 V Si bus also uses a high current of 661 A, which remains unsafe. In recent times, several instances of vehicle catching fire due to high current in batteries have been reported [18]. This could be logical at this point due to the short design of the cable minimizing physical stress on the consumer while charging. On the other hand, Porche Taycan achieves a peak charging power of 270 kW with a maximum charging current of 340 A [13]. Nonetheless, for fair comparison, we have limited the current to 600 A for both the models. Parameters used in this paper are given in Table 3.

Table 3 Battery Parameters for 800 V BEV [18].

Type	No of series connected cells	BMS Cost	Cable and equipment rating
800 V Si	180	2*(592$)	800 V
800V SiC	192	1.3*(818$)	900 V

The charger power input P_{in} and charger power output P_{out} are given below:

$$P_{in} = \sum_{i=1}^{N} \int_{t_s}^{t_s+t_c} I_{DC}\,(t)\,dt \tag{1}$$

$$P_{out} = \sum_{i=1}^{N} \int_{t_s+t_c}^{t_s+t_c+t_d} I_{DC}\,(t)dt \tag{2}$$

Here t_s, t_c and t_d, N are charge start time, charging time, discharging time and number of cycles of AC power during charging respectively. The difference between input and output power is the loss encountered due to higher charging current. For passenger EV, the results are shown in Figure 4.

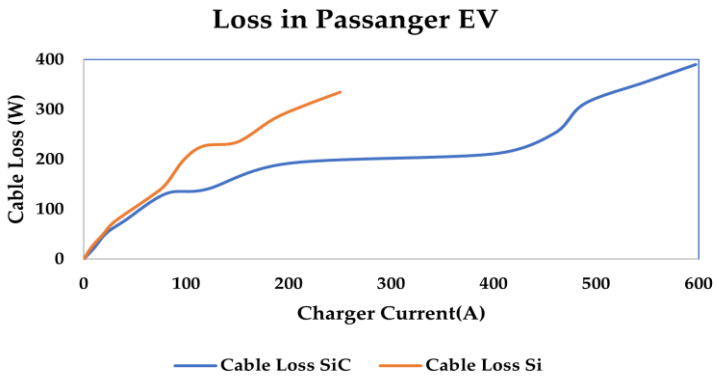

Figure 4 Cable loss for passenger vehicle using 800 V BESS.

A similar approach with higher power components was used to get the output for heavy duty vehicles. These results are shown in Figure 5.

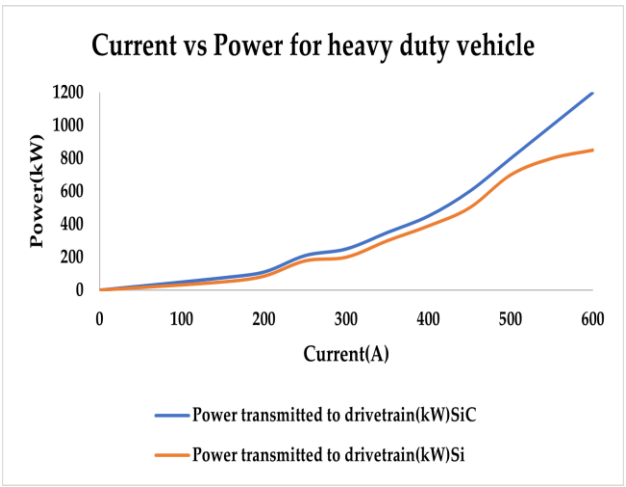

Figure 5 Cable loss for heavy-duty vehicle using 800 V BESS.

The replacement of SiC also increases the State of Health (SoH) of the battery due to the lesser exposure to heat. The battery loses its health due to two types of aging, calendar aging and cycle aging [7]. To calculate these losses a semi empirical formula for total loss [8] is given below.

$$Q^{\,total\ loss}(\delta t) = B_1 e^{B2Irate} I_{rate}\delta t + 0.5 f e^{-\frac{Ea}{RTb}} t^{-\frac{1}{2}} \delta t \qquad (3)$$

where, B_1 & B_2 = polynomials of the temperatures of the battery
T_b = temperatures of the battery.
I_{rate} = rate of current for charging the battery and
R = temperature coefficient.

It is obvious from equation (3) that total loss of power is largely dependent upon temperature. The temperature is directly related to voltage level of the BESS. Therefore, the enhancement of BESS will age the battery faster if the heat dissipation is not controlled. The loss is calculated over a different time period to observe the SoH using the Si and SiC power electronics for powertrain. The results are shown in Table 4.

Table 4 Comparison of State of Health for an 800 V BESS using SiC and Si.

Development in State of Health (SoH) (%) with charging with a 800 V BESS				
0-3/Month		>3/Month		Battery Age (Months)
Si	SiC	Si	SiC	
0.92	0.95	0.88	0.90	3
0.88	0.90	0.84	0.88	6
0.845	0.88	0.78	0.85	12
0.81	0.85	0.75	0.82	24
0.77	0.83	0.72	0.79	36
0.72	0.81	0.69	0.75	48

Table 3 shows improved results with SiC based power electronics. So we see a significant increase in SiC based algorithms. However, it is a tradeoff with the additional monitoring and computational complexity for the higher-powered battery management system (BMS). The pack voltage also impacts SoH as mentioned before and in turn reliability. Despite all these facts it is a fair tradeoff in terms of reliability and customer convenience.

5. Power Electronics

The reduction of power loss in switching devices comes with a twofold benefit. First, reduction of the losses enhances power conversion efficiency and the reduction of cooling components. For small systems the power loss reduction in switching devices might not be significant but for higher power vehicles such as heavy-duty trucks the power loss reduction is very important in terms of both power conversion efficiency and cooling reduction practices. Hence the implementation of SiC is very important for higher power electric vehicles. This might also unfold the possibility of air-cooling instead of liquid cooling in passenger vehicles [19, 20]. In this section we will evaluate the power loss in 800 V powertrain for two most important power electronics components as follows.

5.1 Inverter

In BEV (or PHEV or HEV), the output of the battery is converted into AC by an inverter and fed to the induction motor or permanent magnet synchronous motor. In case of brushless DC electric motor (BLDC) or permanent magnet DC motor (PMDC) a DC-DC converter is used to smoothen the output of the battery [7]. Here the focus remains to compare the electrical performance of the Si and SiC powered 800 V powertrain. We have selected the most used topology, i.e. the 2 level, 3-phase voltage source inverter (VSI) [21]. The center of focus remains the power loss in switching devices during the conversion as known as conduction losses and switching losses. Apart from the current and voltage rating, the power loss also depends on the switching techniques of the converter. Sinusoidal pulse width modulation (SPWM) and space vector pulse width modulation (SVPWM) are the most commonly used switching techniques due to their robust approach [2].

The conduction loss in MOSFET is given by [20],

$$P_{cond} = R_{on}.I^2.(\frac{1}{8} + \frac{M\cos\phi}{3\pi}) \quad (4)$$

The conduction loss [18] in Diode is given by,

$$P_{cond} = \frac{1}{2}(V_D.\frac{1}{\pi} + R_{on}\frac{I^2}{4}) - M\cos\phi(V_D.\frac{1}{8} + R_{on}\frac{2\pi}{3}) \quad (5)$$

where, in equation (4), P_{cond} is the power during the ON state of the MOSFET, R_{on} is the on-state resistance, I the on-state current, M is the modulation index and cosϕ is the power factor. For diode equation of (5), the notations remain the same added with VD as the diode voltage drop.

The power loss has been calculated in 100 kHz and 400 kW output devices. The charging time as a function of charging power for both Si and SiC power electronics is shown in Figure 6. For all values of charging power, lower charging time is obtained for SiC power electronics. This scalable design can be extended till 1.2 GW for the heavy-duty chargers.

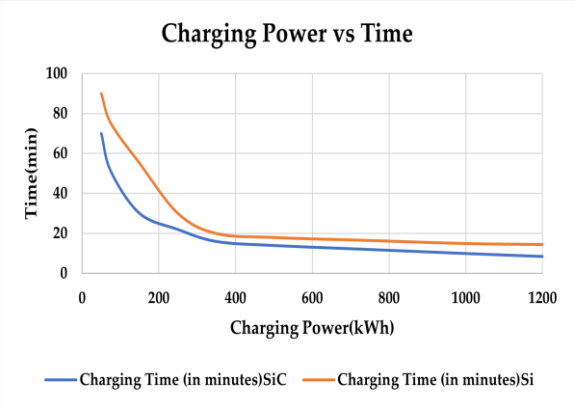

Figure 6 Reduction in charging time due to increase in inverter output.

For the other less used topologies the advantages and disadvantages are listed in Table 3 in reference [20].

5.2 DC-DC Converter

The DC-DC converter is crucial as its function remains to smoothen the flow between Li-ion battery and motor and in case of DC motors, it replaces the inverters. A non-isolated topology used for powertrain has been depicted in Figure 7. It roughly comprises of 30-40% of the total converter weight depending upon the machine used at the end [20, 21]. The individual chip area however is larger than inverter; therefore, despite being smaller the losses are accountable in total. This also brings attention to the fact that due to the denser packaging technology of SiC converters, it is evident that they are a better fit in terms of weight and size for DC-DC converters in traction powertrains. The loss calculation for DC-DC converter is done using a similar approach as in previous sections. The power loss is calculated during ON time of the IGBT and the equations below are fed into the simulator.

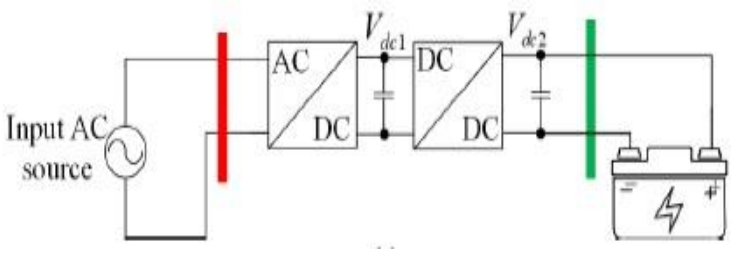

Figure 7 non-isolated DC/DC converter [20].

$$P_{COND} = (V_D I_L + R_{on} I_L^{\,2})(1-D) \tag{6}$$

$$P_{sw} = f_{sw} E_{TT} \frac{V.I}{V_{nom}.I_{nom}} \tag{7}$$

Where the P_{cond} is the power during conduction cycle, P_{sw} is the power during switching of the device, f_{sw} the switching frequency, E_{TT} the reverse recovery emf, V_{nom} and Inom the nominal current and voltage respectively.

Using equations (6) and (7) the loss can be shown in this graph in Figure 8. The blue region denotes the MOSFET conduction and the orange region denotes the diode conduction for the MOSFET+DIODE duo used in the DC-DC converter. Visibly, the conduction is higher in the SiC counterpart.

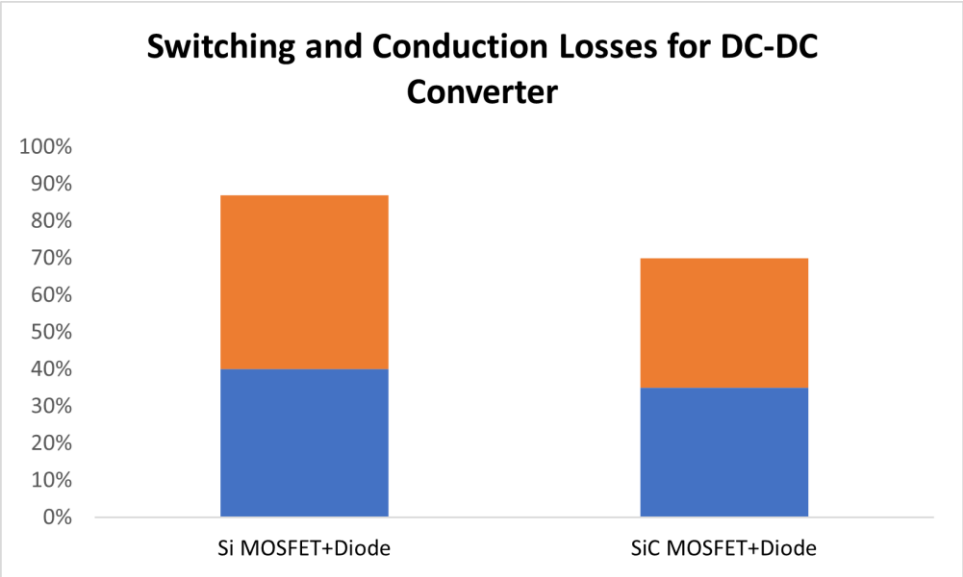

Figure 8 DC/DC converter component loss comparison.

5.3 Enhancement in Motor Output

The enhancement in powertrain design boosts the output of the motor as well. For any given design of machine, the speed of motor increases proportionally to the DC link bus voltage. The induction motor starting torque is given by [22],

$$\text{Starting } T_i = \frac{3}{2\pi N_S} \times \frac{E_2^2 R_\phi}{R_\phi^{\,2} + X_\phi^{\,2}} \tag{8}$$

$$\text{Running } T_R = \frac{3}{2\pi N_S} \times \frac{sE_2^2 R_\phi}{R_\phi^{\,2} + (sX_\phi)^2} \tag{9}$$

$$\text{Average } T_T = \frac{3k^2}{2\pi N_S} \times \frac{sE_1^2 R_\phi}{R_\phi^{\,2} + (sX_\phi)^2} \tag{10}$$

- s = slip of the motor
- E_1 = stator voltage or input voltage
- E_2 = Rotor EMF per phase at a standstill
- R_ϕ = Rotor Resistance Per Phase
- X_ϕ = Rotor Reactance Per Phase
- K = rotor/stator turn ratio per Phase

The performance improvement by evaluating these equations and the model of Figure 2 was used to calculate the output power as a function of inverter power loss. As shown in Figure 9, the SiC inverter operates to a higher operating point with a lesser loss compared to Si counterpart.

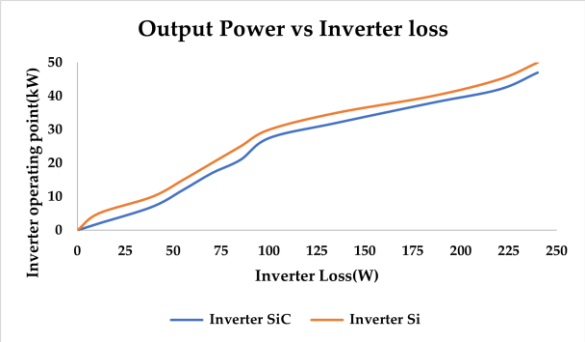

Figure 9 Output Power vs Inverter loss for Motor.

6. Mechanical Constraints

For the same power rating the increase in voltage rating reduces the current rating. Therefore, the cable cross sectional area reduces [23]. As Ohm's law states, lower current reduces copper loss significantly. But increased number of series conductors are required with increased voltage level in turn increasing phase resistance [20]. A higher DC link voltage can help reduce the copper loss and increase the efficiency [23]. In case of a higher-power motor, the iron loss, mechanical loss, and copper loss will increase with revolutions per minute (RPM). Along with the thermal constraints the challenge of mechanical loss must be considered. The rotational speed is the square root of the mechanical loss [24]. Improvement in machine structure such as adding notches or thickening the teeth of the motor may be used. However these in turn increase the complexity in machine design in turn compromising the electromagnetic performance due to the modified rotor structure. Therefore a robust motor model suitable for different traction application is highly desirable.

However with the use of SiC power electronics the stress in motor will be reduced due to lower thermal exposure. Hence all these limitations can be avoided with an 800 V SiC design.

7. Charger Connector Port in 800 V Powertrain for DCFC(Direct Current Fast Charging)

The 250 kW range of charging needs the power electronics to be updated at the end to be capable of charging from the increasing range of level 3 charging. Although 50 kW inwards is considered level 3 DC fast charging, however Tesla Supercharger uses 250 kW in its V3/V4 Supercharger posts. Companies like Tritium are producing 350 kw+ chargers [25]. The currently used topology for charger connector is shown above. The voltage rating of the diode bridge increases with higher charging levels and cost increases. One way to reduce the cost is to adjust the transformer turns ratio thus making it capable of charging from smaller level of grid voltage and the level 3 chargers both. However, the primary focus of this paper remains DC-XFC. Therefore changing the power electronics from Si to SiC remains a plausible solution. It must be noted that the battery pack in 800 V EVs are series connected Li-ion cells that also combat the problem of overheating at high voltage [26]. As stated in reference [26]. Hyundai Ioniq 5 uses a 800 V powertrain with Infineon chips that are combination of SiC and Si power modules [26]. A modified DC-DC topology for grid charging is shown in Figure 10.

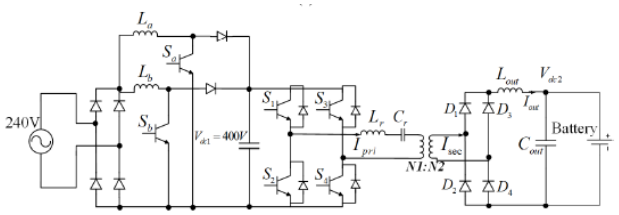

Figure 10 Modified DC/DC topology for grid charging of 800 V vehicles [27].

8. Auxiliary Power Unit (APU)

Zero-voltage-switching full-bridge, full-bridge center-tapped and Dual active bridge converters are the primary topologies used in auxiliary power converters in APU. The APU controls the battery, motor and regulates the voltage level through converter signals. A conventional APU is shown in Figure 11. As the power converter rating increases with the implementation of SiC MOSFET, the need for a component with high enough blocking voltage also arises. Si MOSFETS above 800 V is available in market with the tradeoff of cost and high losses. Instead IGBTs can be used but suffers similar problems of high cost and high turn off time. To reduce the weight and size of passive components such as transformers and capacitors a high frequency (e.g. 100 kHz) device must be chosen, since IGBTs are not suitable for operation above 20 kHz. Keeping all these in mind the SiC MOSFETS emerge as a winner [28]. Implementing SiC will reduce the cooling of the APU by using soft switching in the designated power converter.

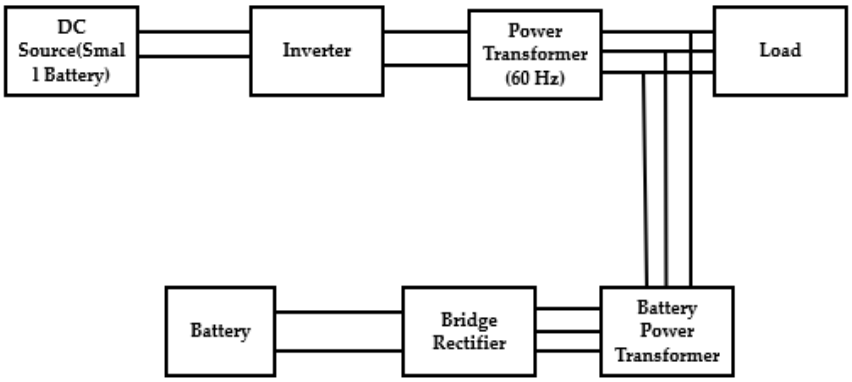

Figure 11 Conventional APU for Powertrains with bulky transformers and Si Electronics [28].

As observed in Table 1 already, SiC has 8 times larger breakdown field compared to Si. Thus, a larger breakdown voltage can be applied in SiC device without increasing the on-state resistance. As the thermal conductivity is also 3 times larger the heat dissipation is more. The wide energy band gap stops the electrons to move to the conduction band making the leakage current lower even in higher temperatures. Furthermore, replacing the conventional IGBT structure of APUs with higher switching frequency of MOSFETS the operation range increases. In certainty the overall APU performance increases.

9. Cost of SiC Power Electronics

All the aforementioned sections give an in-depth look into the high efficiency of SiC and it's potential to replace Si in entire EV structure. However, the current high cost is a major factor obstructing industry to reap the full benefits of SiC. Around 30% to 40% of the cost of the EV inverter pertains to the devices used to build the powertrain. Hence using a device multiple times, higher cost drives the car cost significantly. However, the implementation of SiC will drive down the cost of cooling cost significantly. Thus, reducing the cost. Other than approaches taken during car manufacturing, there are measures to be taken in SiC manufacturing as well. The element of SiC die is abundant in nature, hence, supply chain issues are insignificant. Government's energy policies in favor of electrification of transportation, volume manufacturing and single wafer processing and large diameter wafer manufacturing are being implemented. [29] 200 mm fabs increasing from150 mm are being adopted. This will help to reduce the feature size and defect density of the transistor. The cost of power electronics will also thus reduce just like the reduction of cost of Si. Analogous to the growth of nanoelectronics and power electronics with the implementation of Si instead of rare earth material, the path to SiC will advance in a comparable way. Cost breakdown of a SiC MOSFET die [6] shows that SiC die manufacturer purchased SiC wafer from the market. On the other the hand, data on the right side shows in-house manufacturing of SiC wafer as well as die [6]. Clearly, the cost lowers when companies volume manufacture in their own facility. Thus the substrate cost, die cost and die size can also be reduced.

10. Simulink Design of a Fully SiC Powertrain

To validate the findings of the mathematical model a simulation model was developed. A Li-ion battery block was chosen from Simscape specialized power systems. It was an 800 V battery which is capable of running a multi motor system. A 3 ph neutral point clamped converter is used using the SiC MOSFET Mitsubishi PSF25S92F6-A. The switching control was done akin to the grid tie inverter switching using MPC. The applied method is used for obtaining optimal switching sequence (OSS) concept to compute the control action. The system constraints like temperature and current limit need to be handled by the simulation model. Therefore, the computational burden needs to be in a certain limit. In many digital hardware platforms this method is implemented nowadays. OSS applies the switching sequence to the power converter during the next sampling period. However, PWM may seem like a more robust and conventional option, but the purpose of this paper lies in the justification of power savings by SiC implementation and the faster switching time and higher current limit of SiC can handle the higher-level control algorithm [29]. The load chosen is a fixed RL load.

The switching sequence for 3^3 or 27 switches were manually computed as mentioned in Table 5. Using the forward Euler's method in voltage equation the reference block was created. For a RL load the working equation can be given by

$$\frac{di_s}{dt} = \frac{1}{L}(v_s - ri_s - v_{ab}) \tag{11}$$

The equation uses a for loop and repeats the action for the corresponding switching signal. This code was placed inside a MATLAB function block and the result was used as the switching signal for Neutral Point Clamp Converter. The switching states are shown in Table 5.

Table 5 switching sequence for the respective legs of the neutral point clamped converter.

M1X	ON	OFF	OFF
M2X	ON	ON	OFF
M3X	OFF	ON	ON
M4X	OFF	OFF	ON
VXO	VDC	0	VDC
Switching States	1	0	-1

Following the switching states as mentioned above the vectors for 3^3 or 27 switching sequences were calculated manually and put into the function block working as the trigger circuit for the Powertrain converter. The switching sequences are mentioned in Table 6.

Table 6 Calculated switching sequence for the proposed model.

Vector	M_a	M_b	M_c
V_0	-1	-1	-1
V_1	0	0	0

V_2	1	1	1
V_3	1	0	0
V_4	0	-1	-1
V_5	0	0	-1
V_6	1	1	0
V_7	0	1	-1
V_8	-1	0	-1
V_9	-1	0	0
V_{10}	0	1	1
V_{11}	0	0	1
V_{12}	-1	-1	0
V_{13}	0	-1	0
V_{14}	1	0	1
V_{15}	1	-1	-1
V_{16}	1	0	-1
V_{17}	1	1	-1
V_{18}	0	1	-1
V_{19}	-1	1	-1
V_{20}	-1	1	0
V_{21}	-1	1	1
V_{22}	-1	0	1
V_{23}	-1	-1	1
V_{24}	0	-1	1
V_{25}	1	-1	1
V_{26}	1	-1	0

The Simulink model can be expressed in terms of block diagram as shown in Figure 12. Battery is connected to the block that covers all the references defined under the reference block. The function block carries the switching sequence and equations in a *for* loop to act as the switching circuit. The signals then trigger the MOSFETS in the Neutral point clamp converter according to the switching table, sequentially connected to the fixed RL load. The generated voltage that could be seen in the scope.

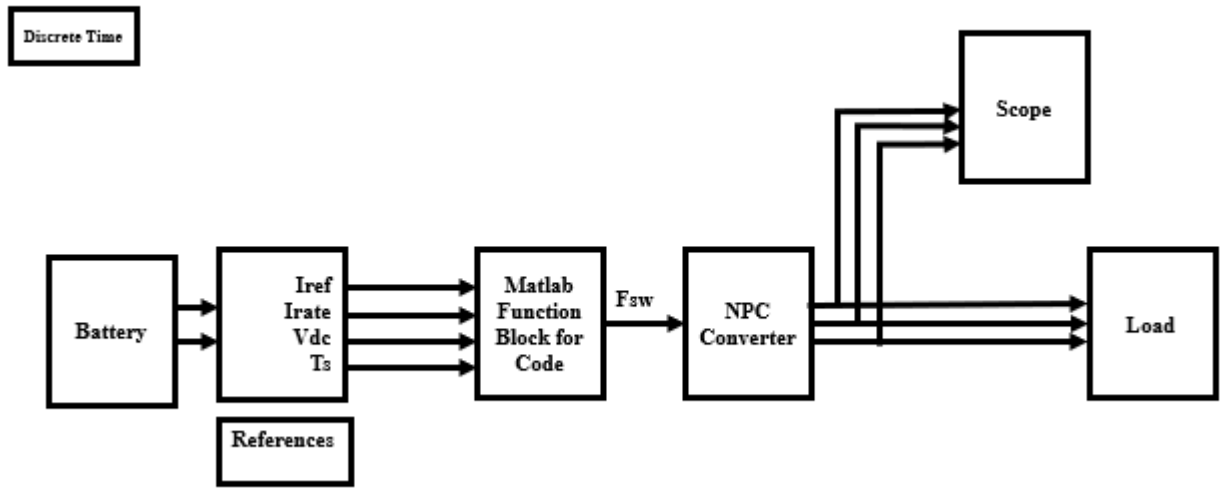

Figure 12 Block Diagram of Developed Simulation Model.

The power output for one motor system can be seen below in Figure 13. Three phases are depicted separately in Figure 13 (a). On the other hand, Figure 13 (b) depicts three phases simultaneously in different colors for ease of understanding. This is a scalable design suitable for any upgraded power electronics for the future. Another smaller motor can be connected at the battery output as the higher efficiency SiC is wasting less battery power and working at its optimal output level.

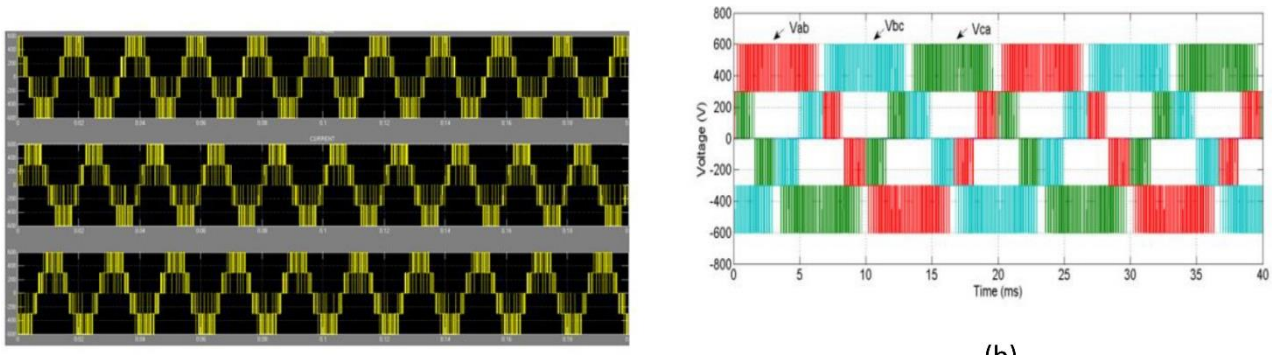

(a) (b)

Figure 13 (a)Simulation result for output voltage of SiC-NPC converter- three separate phases. (b)Simulation result for output voltage of SiC-NPC converter- three phases simultaneously.

11. Conclusion

In this article we have analyzed the future trend in EVs to completely switching to SiC based power electronics-based power train instead of the current use of Si power electronics for higher voltage levels. A similar 800 V Si power train system derived mathematically and by simulation was compared to the SiC power electronics-based system. A thorough step by step analysis for all the components of powertrain was done. The findings show that even with a similar 800 V battery the

size and mass reduction due to the reduction in cooling components and higher current carrying capability remains significant. The motor of the power train can achieve more RPM under SiC technology. The power electronics will be lighter and heat dissipation will be significantly lower. The chargers will have a robust structure under SiC to enable faster charging in both grid connected and DC fast charger mode. Even the smaller components used in auxiliary power unit will show a stark reduction in size and power density due to replacement with SiC enabled bus. With the cost reduction trend of silicon carbide power electronics, our conclusion is that the power level can be significantly increased to keep up with the ever-increasing capacity of extremely fast charging thus attracting more customers for electric vehicles.

Author Contributions

Conceptualization: N.D. and R.S. Research, Simulation and Result Processing: N.D, review and editing: N.D and R.S.; supervision, R.S.; project administration, R.S. All authors have read and agreed to the published version of the manuscript.

Competing Interests

The authors have declared that no competing interests exist.

References

1. Opinion: Antarctica's riskiest glacier is under assault from below and losing its grip, threatening to raise sea levels by 10 feet [Internet]. Available from: https://www.marketwatch.com/story/antarcticas-riskiest-glacier-is-under-assault-from-below-and-losing-its-grip-threatening-to-raise-sea-levels-by-10-feet-11654717813.
2. Mobility's net-zero transition: A look at opportunities and risks [Internet]. Available from: https://www.mckinsey.com/industries/automotive-and-assembly/our-insights/mobilitys-net-zero-transition-a-look-at-opportunities-and-risks?cid=other-eml-alt-mip-mck&hlkid=8ce86e4f93394d5792c812d309e9d0d5&hctky=13415767&hdpid=3bcb779a-4a61-43ff-b6ef-7cad705e48a.
3. Oil has long been used as a geopolitical weapon. Could electrified transport change that? [Internet]. Toronto: CBC. Available from: https://www.cbc.ca/news/electric-vehicles-oil-transition-1.6434080.
4. Singh R, Paniyil P, Zhang Z. Transformative role of power electronics: In solving climate emergency. IEEE Power Electron Mag. 2022; 9: 39-47.
5. Lambert F. Global market share of electric cars more than doubled in 2021 as the EV revolution gains steam [Internet]. Available from: https://electrek.co/2022/02/02/global-market-share-of-electric-cars-more-than-doubled-2021/.
6. The world's electric vehicle fleet will soon surpass 20 million [Internet]. Available from: https://www.bloomberg.com/news/articles/2022-04-08/plug-in-ev-fleet-will-soon-hit-a-20-million-milestone.
7. Deb N, Singh R, Brooks RR, Bai K. A review of extremely fast charging stations for electric vehicles. Energies. 2021; 14: 7566.

8. Deb N, Singh R. An analysis of SiC power electronics implementation in green energy based extremely fast charging. J Eng Res Sci. 2022; 1: 231-242.
9. Voelcker J. Porsches 800-volt fast charging for electric cars: Why it matters [Internet]. 2020. Available from: https://www.greencarreports.com/news/1106954_porsches-800-volt-fast-chargingfor-electric-cars-why-it-matters.
10. Most of the EV industry to shift to 800 volts by 2025, report says [Internet]. Available from: https://insideevs.com/news/580829/ev-industry-shifting-to-800-volt-2025/#:~:text=Right%20now%2C%20only%20a%20handful,architecture%20created%20with%20proprietary%20tech.
11. Jung C. Power up with 800-V systems: The benefits of upgrading voltage power for battery-electric passenger vehicles. IEEE Electr Mag. 2017; 5: 53-58
12. Küpper K, Pels T, Deiml M, Angermaier A, Bürger T, Weinzerl A, et al. Tension 12 V to 800 V efficient powertrain solutions [Internet]. AVL; 2020. Available from: http://siar.ro/wp-content/uploads/2016/01/2.-Kupper-K.-AVL-Tension-12-V-to-800-V-2015.compressed.pdf.
13. Aghabali I, Bauman J, Kollmeyer PJ, Wang Y, Bilgin B, Emadi A. 800-V electric vehicle powertrains: Review and analysis of benefits, challenges, and future trends. IEEE Trans Transp Electrification. 2020; 7: 927-948.
14. Qorvo design summit 2022 [Internet]. Available from: https://unitedsic.com/products/sic-fets/uf3c170400k3s/infineon.com/dgdl/Infineon-IPD80R2K7C3A-DS-v01_01-EN.pdf?fileId=5546d4625e763904015ec2d9c72064a0.
15. Vehicle modeling R2018a (Fixed Loop Error) [Internet]. Available from: https://github.com/mathworks/vehicle-modeling/releases/tag/v4.1.1.
16. Andwari AM, Pesiridis A, Rajoo S, Martinez-Botas R, Esfahanian V. A review of Battery Electric Vehicle technology and readiness levels. Renew Sust Energ Rev. 2017; 78: 414-430.
17. A Tesla burst into flames while charging and spread to a nearby home [Internet]. Available from: https://www.motorbiscuit.com/tesla-burst-flames-charging-spread-nearby-home/.
18. EV design – battery calculation [Internet]. Available from: https://x-engineer.org/ev-design-battery-calculation/.
19. Shang F, Arribas AP, Krishnamurthy M. A comprehensive evaluation of SiC devices in traction applications. 2014 IEEE Transportation Electrification Conference and Expo (ITEC). IEEE; 2014.
20. Poorfakhraei A, Narimani M, Emadi A. A review of multilevel inverter topologies in electric vehicles: Current status and future trends. IEEE Open J Power Electron. 2021; 2: 155-170.
21. Induction motor & linear induction motors formulas & equations [Internet]. Available from: https://www.electricaltechnology.org/2020/10/linear-induction-motor-formulas-equations.html.
22. Thermal management in the silicon carbide revolution [Internet]. Available from: https://www.idtechex.com/en/research-article/thermal-management-in-the-silicon-carbide-revolution/24961.
23. Dabala K. Analysis of mechanical losses in three-phase squirrel-cage induction motors. ICEMS'2001. Proceedings of the fifth international conference on electrical machines and systems (IEEE Cat. No. 01EX501). IEEE; 2001.
24. Abbasi M, Lam J. An SiC-based AC/DC CCM bridgeless onboard EV charger with coupled active voltage doubler rectifiers for 800-V battery systems. 2020 IEEE applied power electronics conference and exposition (APEC). IEEE; 2020.

25. 400v vs 800v what's the difference? Electric car battery voltage explained [Internet]. Available from: https://www.carsguide.com.au/ev/advice/400v-vs-800v-whats-the-difference-electric-car-battery-voltage-explained-88101.
26. Lee IS, Kang JY, Lee J, Lee ST. Design considerations of auxiliary power supply unit with SiC MOSFET for lightweight railway vehicles. 2018 21st International Conference on Electrical Machines and Systems (ICEMS). IEEE; 2018.
27. Tritium Veefil PK350 [Internet]. Available from: https://smartchargeamerica.com/electric-car-chargers/commercial/tritium-veefil-pk350/.
28. Wolfspeed opens the world's largest 200mm silicon Carbide fab enabling highly anticipated device production [Internet]. Available from: https://investor.wolfspeed.com/news/news-details/2022/Wolfspeed-Opens-the-Worlds-Largest-200mm-Silicon-Carbide-Fab-Enabling-Highly-Anticipated-Device-Production/default.aspx.
29. Vázquez Pérez S, P Aguilera R, Acuna P, Pou J, León Galván JI, García Franquelo L, et al. Model predictive control for single-phase NPC converters based on optimal switching sequences. IEEE Trans Ind Electron. 2016; 63: 7533-7541.